Nano-opto-mechanically modulated plasmonic nanoantenna-integrated quantum cascade laser

John Kohoutek, Dibyendu Dey, Alireza Bonakdar, Ryan Gelfand, Vala Fathipour, et al.

John Kohoutek, Dibyendu Dey, Alireza Bonakdar, Ryan Gelfand, Vala Fathipour, Omer Gokalp Memis, Hooman Mohseni, "Nano-opto-mechanically modulated plasmonic nanoantenna-integrated quantum cascade laser," Proc. SPIE 8456, Nanophotonic Materials IX, 84560K (15 October 2012); doi: 10.1117/12.2006932

SPIE.

Event: SPIE NanoScience + Engineering, 2012, San Diego, California, United States

Nano-opto-mechanically modulated plasmonic nanoantenna-integrated quantum cascade laser

John Kohoutek, Dibyendu Dey, Alireza Bonakdar, Ryan Gelfand, Vala Fathipour, Omer Gokalp Memis, Hooman Mohseni

Bio-Inspired Sensors and Optoelectronics Laboratory (BISOL), EECS, Northwestern University, 2145 Sheridan Rd., Evanston, Illinois, USA

ABSTRACT

We report mechanical frequency and amplitude modulation of a quantum cascade laser (QCL) integrated with a plasmonic antenna operating at ~6.1 μm. We have observed a shift in the lasing frequency by over 30 GHz and an intensity modulation of ~74% when an atomic force microscope (AFM) tip approaches the hot spot of a metal-dielectric-metal (MDM) bow-tie antenna integrated onto the facet of the laser. The tip diameter is ~λ/60 and in non-contact mode its amplitude of motion is ~λ/120. We have presented a theoretical model based on the rate equations for a QCL which affirms our experimental observations. Our experiment demonstrates the strong influence of the hot spot on the laser cavity modes, despite the fact that the former is many orders of magnitude smaller than the latter. We have compared our device to a previous mechanically frequency modulated QCL and calculated a figure of merit, change in frequency divided by change in distance of the mechanical component ($\Delta f/\Delta d$), which is an order of magnitude higher, while our design uses a volumetric change per λ^3 that is five orders of magnitude smaller. Our device differs from optical gradient force actuated devices in that our device is externally mechanically actuated while those devices are self actuated through the optical force. This sensitivity of the laser cavity mode to the position of a nanometer-scale metallic absorber opens up the opportunity for modulating large amount of optical power by changing the optical properties of a miniscule volume in an integrated, chip-scale device.

Keywords: QCL tuning, plasmonic nanoantenna, frequency/amplitude modulation, mechanical tuning, MEMS/NEMS, opto-mechanical, nano-opto-mechanical

1. INTRODUCTION

A surface plasmon (SP) is a collective motion of electrons generated by light at the interface between two mediums of opposite signs of dielectric susceptibility (e.g. metal and dielectric) [1]. This principle has recently been exploited in such applications as enhanced optical transmission for photodetection [2, 3], biosensing [4], optical trapping [5, 6]. Recently, there has been increased activity in using SP based devices for optical modulation [7], more specifically including all-optical modulation [8-12]. Furthermore, opto-mechanical coupling and devices have recently been used for such applications as optical modulation and tuning [13-15], optical switching and mux [12, 16], photodetection [17, 18], and force sensing and manipulation [19-21]. One attractive target for SP optical antenna based devices is the quantum cascade laser, because of its many uses [22-25]. The mode of this laser source is very sensitive to the reflectivity of the facets [11, 13, 26], so that by changing the reflectivity of one facet, one achieves a viable way to externally modulate the output. Recently, a method of micro-opto-mechanical QCL tuning has been demonstrated [14]. Here we experimentally demonstrate nano-opto-mechanical QCL tuning, using an alternative approach, where a small change in the position of an atomic force microscope (AFM) tip coupled to a plasmonic nanoantenna tunes the laser frequency as well as its output power [13]. Because we are using the apex of the AFM tip to interact with the antenna hot spot, thus modulating

Nanophotonic Materials IX, edited by Stefano Cabrini, Taleb Mokari, Proc. of SPIE Vol. 8456, 84560K · © 2012 SPIE · CCC code: 0277-786/12/$18 · doi: 10.1117/12.2006932

the entire laser, our approach uses an external volumetric change which is many orders of magnitude less than the previous approach to modulate the laser output [14] mechanically. We have measured the output laser spectrum and amplitude of the device as a function of AFM tip position over the hotspot, as well as measured the near-field image using a modified apertureless near-field scanning optical microscope [24, 25].

2. FABRICATION

Our device has been fabricated by defining a metal-dielectric-metal stacked (MDM) bow-tie antenna structure on the facet of the quantum cascade laser. The antenna is designed and optimized for our laser source using full 3-D finite-difference-time-domain (FDTD) simulations. The bow-tie design consists of two triangle structures separated by a gap of 100 nm. These composite material (MDM) based nano-antennas have showed an improved performance in terms of near field intensity enhancement over single metal designs [24, 25]. After optimizing the design, the MDM bow-tie structure was fabricated on the coated facet of the QCL using a focused ion beam (Hellios FEI). The fabrication details for this device have been described in our previous letters [24, 25]. We have previously optimized the antenna fabrication process such that it reduces the threshold current density by 25% without changing the other laser parameters significantly [11, 24, 25]. This reduction is mainly due to the increased reflectivity of the gold coated facet [25].

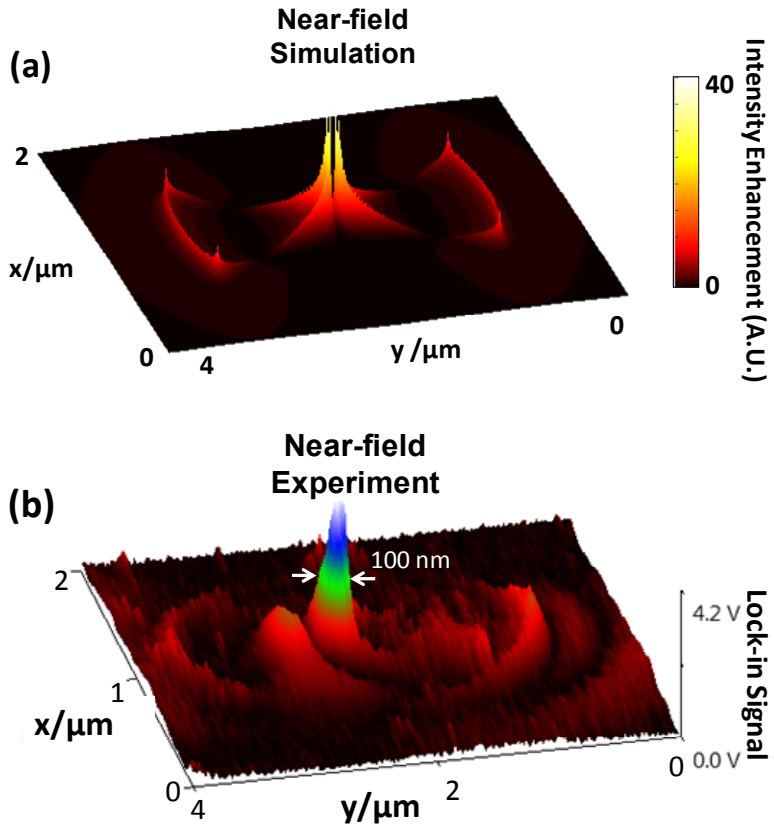

Figure 1 - Near-field image of the bow-tie antenna on the facet of the QCL. (a) - Simulation. (b) Experiment.

3. EXPERIMENT

The plasmonic mode created by the focusing of light by the optical antenna exists only in the near field and thus cannot be studied with an ordinary microscope. Previously, we have used a backscattered apertureless near-field

scanning optical microscope to map the near field of the device (a-NSOM) [27, 28]. For this work, however, we have used a modified a-NSOM, which can also measure the mid-wave infrared spectrum (in the region of operation) of the device with respect to time and vertical and horizontal AFM tip position. Figure 1 shows the simulation and experimental result of the near field produced by the bow-tie antenna.

For the measurement, the laser was pulsed using a voltage pulse generator and enclosed in a temperature and airflow stabilized environment. To record the lasing spectrum at a certain vertical position of the AFM tip, both the voltage pulse generator and an FTIR were synchronized with the AFM tip's vibration frequency via lock-in method. The lock-in amplifier allows for synchronization of these two frequencies in the following way. First, the amplitude signal from the AFM is fed into the reference input of the lock-in. Next, the trigger-out of the lock-in is fed into the trigger-in of the voltage pulse generator. Finally, the high voltage pulse from the voltage pulse generator is used to pulse the QCL device, while the trigger-out signal from the pulse generator is simultaneously used to trigger the FTIR. The FTIR uses an external MCT detector for both the interferogram described below as well as the a-NSOM signal described above.

The voltage pulse generator has a pulse delay mechanism that allows us to vary the delay of the pulse sent to the laser with respect to the AFM trigger signal. In turn, this lets us measure the spectrum at different vertical positions of the AFM tip over the hot spot. The spectrum was recorded at 6 equidistant delay points between 0 and 2π with respect to the AFM tip cycle. As the natural vibration frequency of the AFM tip was measured to be ~ 90 kHz (Ω), each tip position repeated itself at an interval of ~ 11.1 μs (Ω^{-1}). The resolution of the time resolved measurement was kept at 10 ns, thereby recording 5 sets of spectral data for an operating pulse width of 50 ns.

FTIR works on the basis of a simple Michelson interferometer originally developed in 1891. The original beam of light is divided into two paths by a beamsplitter and recombined after travelling down separate path lengths, by reflecting off of one fixed and one moving mirror. After traveling down the separate paths the beams are recombined and fall incident on a detector where they interfere with each other, creating an *interferogram*. Because of the effect of interference, the intensity of each beam passing to the detector depends on the path difference in the two arms of the interferometer. This variation of intensity at the detector ultimately yields the spectral information in a FTIR. The interferogram is created with dimensions of length (cm), so taking the Fourier Transform inverts the dimension, giving units of cm^{-1}, or wavenumber [29].

The time resolved step-scan for all measurements is shown in Figure 2a. As the delay was varied and hence vertical AFM tip position, the central frequency of operation of the laser shifted. The amplitude modulation of this vertical tip movement is shown in Figure 2b. In effect, this has created nano-optical-mechanical frequency and amplitude modulation in the laser device.

4. THEORY

To describe the experimental observation, we have used the rate equations [26] that govern the density of carriers in the upper and lower states of the QCL, photon density, and change in current density near the operating point of our device. The QCL parameters we have used in solving the rate equations are based on published data [30-33] with a similar active region design to ours and show good agreement with the experimental threshold current density of our laser. The rate equations contain a mirror loss term (α_M) which contains the reflectivity of the facet with the constructed antenna, which was found to be changing through FDTD simulations because of the motion of the AFM tip with respect to the antenna. To calculate the change in reflectivity of the bow-tie antenna, we record the electric and magnetic fields near the back of the device and calculate the reflected power with and without the AFM tip over the hot spot to be 12%. We solved the rate equations self consistently for the photon density s, and the state densities of the third and second levels n_3 and n_2 respectively as a function of time for a moving tip. We found that the laser output power can change by a maximum of 93%, while we have observed a change of 74% experimentally. Thus, the amplitude of the laser is also modulated mechanically. The difference between the two figures is likely due to imperfections and real-life conditions with experimental setup and measurement techniques compared to a completely optimized simulation. To calculate the change in frequency as a function of time we have taken the rate carriers that produce heat through different non-

radiative mechanisms from the rate equations, n_3/τ_3 and n_2/τ_2, where τ_3 and τ_2 are the lifetimes of the excited states three and two, respectively, and multiplied them by the respective energy of those transitions as well as the heat losses due to photon absorption in the waveguide. We also included the variation of the Joule heat in the laser due to rapid change of laser current density near threshold at a constant bias [34, 35] which gives a term that is the change of current near threshold times the voltage at our bias point of the QCL (1 percent above threshold) to get the power lost due to heat in the QCL:

$$P_{heat} = V_{cavity} \cdot \left(\frac{n_3}{\tau_3} E_{photon} + \frac{n_2}{\tau_2} 2E_{phonon} + s \cdot E_{photon}^{lost} \cdot \frac{\alpha_W c}{n_{eff}} \right) + \Delta I \cdot V_{app} \qquad (1)$$

Where V_{cavity} is the volume of the active region of the cavity, E_{phonon} is the LO phonon resonance energy (30 meV), multiplied by two because the active region of our design generates two phonons per transition, E_{photon} is the photon energy, ΔI is the change in current near threshold (defined as point of maximum positive second derivative in current-power plot), and V_{app} is the applied voltage. Then, we have calculated the change in core temperature when considering this power term and the thermal resistance of the laser [36-38]:

$$R_{thermal} = \frac{\ln\left(4\frac{h}{w}\right)}{4\pi\xi} \qquad (2)$$

where h is the height of the active region, w is the width, and ξ is the thermal conductivity of the material separating the source from the sink. The core temperature is found to be varying as a function of time, due to the time varying terms in the P_{heat} equation, originally coming from the laser facet change in reflectivity. Finally we have used the relation $\Delta k = \Delta T \cdot k\left(b + a \cdot n_{eff}\right)/n_{eff}$ to find the change in wavenumber as a function of time, and converted to frequency [39]. Here, k is wavenumber in cm^{-1} converted to Δf – frequency in GHz, b is temperature coefficient of change in refractive index (5.9×10^{-4}), and a is linear thermal expansion coefficient (5.54×10^{-6} K^{-1}) [39]. The results of this calculation show a final Δf of 31.8 GHz, in good agreement with our experimental data.

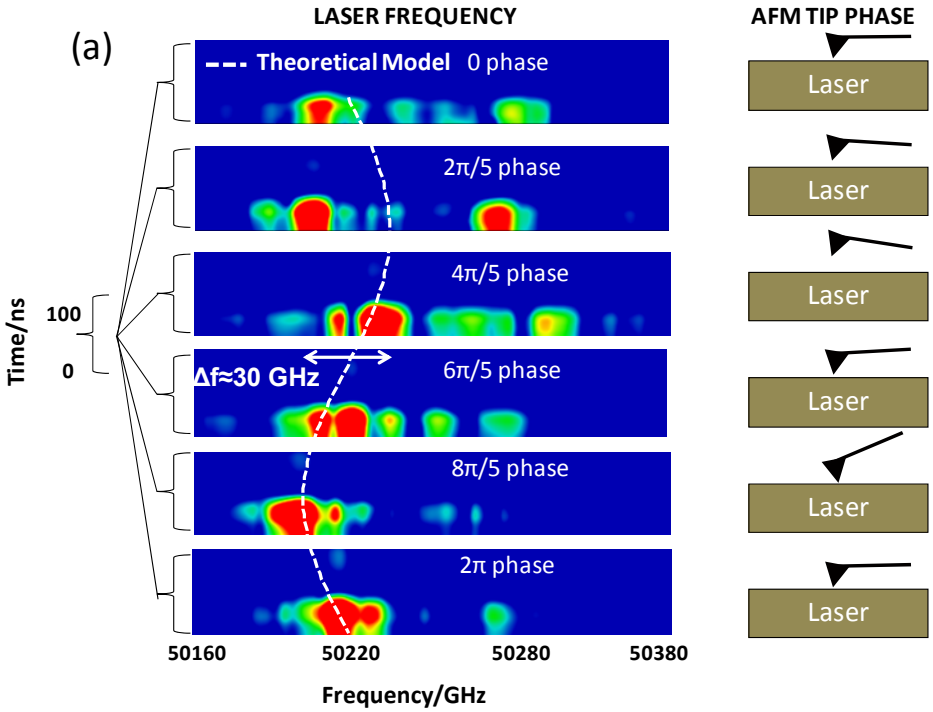

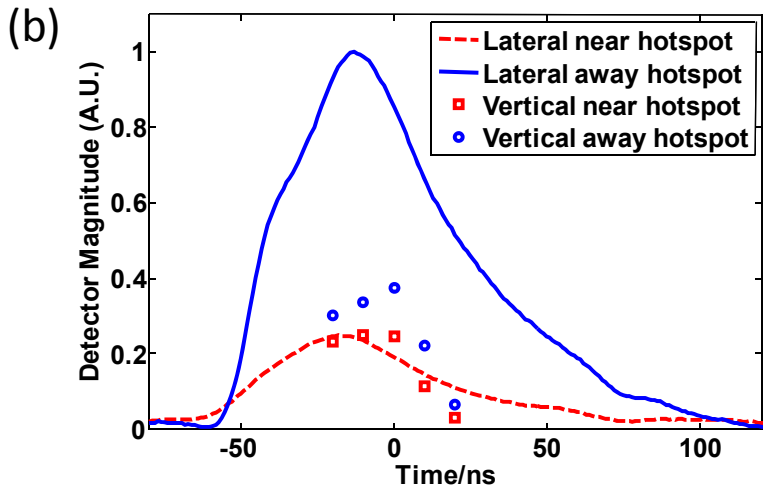

Figure 2 - (a) (previous page) Time resolved step-scan as a function of vertical tip position over the hot spot of the plasmonic nanoantenna on the QCL. (b) Detector signal when AFM tip is moved either vertically or laterally over the nanoantenna hotspot.

5. DISCUSSION/CONCLUSION

The time resolved step-scans as a function of vertical AFM tip position are shown in Figure 2a. The peaks in the figure are normalized so that one can accurately discern the frequency shift in the measurement. There we have recorded the frequency shift when the AFM tip moves with an amplitude of ~50 nm toward and away from the hotspot and recorded a signal amplitude modulation of 33.3% (Figure 2b). We also observed more than 74% laser power variation when an AFM tip is moved towards and away from the hotspot laterally (distance of microns) as shown in Figure 2b. Thus, a small variation of the AFM tip position can change the output of the laser significantly due to the strong coupling of the plasmonic mode to the QCL laser cavity modes. This behavior is very interesting, because without the strong influence of the nano-antenna, the emitted light at λ=6.1 μm would not be significantly scattered by an object that is ~60 times smaller than its wavelength. Also, the motion of such a small scattering point by a small amount (~λ/120) would only lead to an extremely small change of laser output. Without the antenna this interaction would have produced a nearly four orders of magnitude less amplitude change, according to our simulations, a change of only 0.007%.

In non-contact mode operation, the AFM tip has an oscillation amplitude of ~50 nm toward and away from the hotspot, and there is never a point of contact with the surface. We have calculated a figure of merit for the system of change in frequency over change in distance of the mechanical modulator, $g=\Delta f/\Delta d \sim 6.4\times10^{8}$ Hz nm^{-1}. Although the previously mentioned external mechanical frequency tuned QCL show a larger relative tuning range, the g value of the device was on the order of ~2.7×10^{7} Hz nm^{-1} which is an order of magnitude less than what we report here. In parallel, our device requires approximately five orders of magnitude less mechanical volumetric change per λ^3. While the previous device requires a micro-scale object and range of motion [14], our device requires a nanometer scale object (radius of curvature of tip) and range of motion (amplitude of vibration of tip) [13]. We believe that the reason for the higher g in our device versus the previous is the high mode confinement via the plasmonic nanoantenna and the strong coupling of that mode to the cavity mode of the QCL. When the plasmonic mode is modified by the AFM tip, it strongly changes the cavity mode of the laser through this strong coupling. These externally mechanically actuated devices differ from previous designs that use the optical gradient force to modulate the frequency [21], because those devices use the optical gradient force to actuate themselves.

In conclusion, the laser cavity mode has shown an extremely high sensitivity with respect to the position of the AFM tip over the nanoantenna hotspot. The laser power is reduced by ~ 74% and shifts by nearly 30 GHz with a change in the AFM tip position near the hot-spot, creating nanomechanical frequency and amplitude modulation. A theoretical model was developed based on laser rate equations and dynamic mirror reflectivity that confirm our experiments. This strong coupling relies on a metal-dielectric-metal plasmonic bow-tie antenna integrated onto the facet of a QCL which can squeeze the optical mode to within a spot size of ~ 100nm – this is 60 times smaller than the operating wavelength. We used finite-difference-time-domain (FDTD) software to optimize the design of such a device and measured it using a modified apertureless near-field scanning optical microscope (a-NSOM). This setup can measure amplitude and spectrum of the device as a function of time and AFM tip position simultaneously. We have compared our device to a previous frequency modulated QCL [14] and shown a figure of merit *g* which is an order of magnitude higher while our design uses a mechanical volumetric change per λ^3 that is five orders of magnitude smaller than the previous design. Our device differs from previous optical force actuated devices in that our device is externally mechanically actuated while those devices are self actuated through the optical force [21]. This demonstration of a nano-opto-mechanical frequency and amplitude modulation in the terahertz region of the spectrum opens up the opportunity for modulating large amount of optical power by changing the optical properties of a miniscule volume in an integrated, chip-scale device.

6. REFERENCES

[1] H. Raether, [Surface plasmons on smooth and rough surfaces and on gratings] Springer, New York(1988).

[2] T. W. Ebbesen, H. J. Lezec, H. F. Ghaemi, T. Thio, and P. A. Wolff, "Extraordinary optical transmission through sub-wavelength hole arrays," Nature, 391(6668), 667-669 (1998).

[3] W. Wu, A. Bonakdar, and H. Mohseni, "Plasmonic enhanced quantum well infrared photodetector with high detectivity," Applied Physics Letters, 96(16), (2010).

[4] R. M. Gelfand, L. Bruderer, and H. Mohseni, "Nanocavity plasmonic device for ultrabroadband single molecule sensing," Optics Letters, 34(7), 1087-1089 (2009).

[5] M. Righini, A. S. Zelenina, C. Girard, and R. Quidant, "Parallel and selective trapping in a patterned plasmonic landscape," Nature Physics, 3(7), 477-480 (2007).

[6] M. Righini, P. Ghenuche, S. Cherukulappurath, V. Myroshnychenko, F. J. G. de Abajo, and R. Quidant, "Nano-optical Trapping of Rayleigh Particles and Escherichia coli Bacteria with Resonant Optical Antennas," Nano Letters, 9(10), 3387-3391 (2009).

[7] M. J. Dicken, L. A. Sweatlock, D. Pacifici, H. J. Lezec, K. Bhattacharya, and H. A. Atwater, "Electrooptic Modulation in Thin Film Barium Titanate Plasmonic Interferometers," Nano Letters, 8(11), 4048-4052 (2008).

[8] R. A. Pala, K. T. Shimizu, N. A. Melosh, and M. L. Brongersma, "A nonvolatile plasmonic switch employing photochromic molecules," Nano Letters, 8(5), 1506-1510 (2008).

[9] N. Large, M. Abb, J. Aizpurua, and O. L. Muskens, "Photoconductively Loaded Plasmonic Nanoantenna as Building Block for Ultracompact Optical Switches," Nano Letters, 10(5), 1741-1746 (2010).

[10] J. A. Dionne, K. Diest, L. A. Sweatlock, and H. A. Atwater, "PlasMOStor: A Metal-Oxide-Si Field Effect Plasmonic Modulator," Nano Letters, 9(2), 897-902 (2009).

[11] J. Kohoutek, A. Bonakdar, R. Gelfand, D. Dey, I. H. Nia, V. Fathipour, O. G. Memis, and H. Mohseni, "Integrated All-Optical Infrared Switchable Plasmonic Quantum Cascade Laser," Nano Letters, 12(5), 2537-2541 (2012).

[12] A. Bonakdar, J. Kohoutek, D. Dey, and H. Mohseni, "Optomechanical nanoantenna," Optics Letters, 37(15), 3258-3260 (2012).

[13] J. Kohoutek, D. Dey, A. Bonakdar, R. Gelfand, V. Fathipour, O. G. Memis, and H. Mohseni, "Mechanical frequency and amplitude modulation of quantum cascade laser integrated with plasmonic nanoantenna," Small, (2012).

[14] Q. Qin, B. S. Williams, S. Kumar, J. L. Reno, and Q. Hu, "Tuning a terahertz wire laser," Nature Photonics, 3(12), 732-737 (2009).

[15] M. Eichenfield, C. P. Michael, R. Perahia, and O. Painter, "Actuation of micro-optomechanical systems via cavity-enhanced optical dipole forces," Nature Photonics, 1, 416-422 (2007).

[16] Z. F. Wang, W. Cao, X. C. Shan, J. F. Xu, S. P. Lim, W. Noell, and N. F. de Rooij, "Development of 1x4 MEMS-based optical switch," Sensors and Actuators a-Physical, 114(1), 80-87 (2004).
[17] J. Kohoutek, I. Y. L. Wan, O. G. Memis, and H. Mohseni, "An opto-electro-mechanical infrared photon detector with high internal gain at room temperature," Optics Express, 17(17), 14458-14465 (2009).
[18] B. Belier, A. Santoso, J. Bonnafe, L. Nicu, P. Temple-Boyer, and C. Bergaud, "Micro-optomechanical sensor for optical connection in the near field," Applied Physics Letters, 77(12), 1768-1770 (2000).
[19] J. Kohoutek, D. Dey, A. Bonakdar, R. Gelfand, A. Sklar, O. G. Memis, and H. Mohseni, "Opto-mechanical force mapping of deep subwavelength plasmonic modes," Nano Letters, 11(8), 3378-82 (2011).
[20] G. Volpe, R. Quidant, G. Badenes, and D. Petrov, "Surface plasmon radiation forces," Physical Review Letters, 96(23), (2006).
[21] D. Van Thourhout, and J. Roels, "Optomechanical device actuation through the optical gradient force," Nature Photonics, 4(4), 211-217 (2010).
[22] N. Yu, E. Cubukcu, L. Diehl, M. A. Belkin, K. B. Crozier, F. Capasso, D. Bour, S. Corzine, and G. Hofler, "Plasmonic quantum cascade laser antenna," Applied Physics Letters, 91(17), (2007).
[23] N. Yu, E. Cubukcu, L. Diehl, D. Bour, S. Corzine, J. Zhu, G. Hoefler, K. B. Crozier, and F. Capasso, "Bowtie plasmonic quantum cascade laser antenna," Optics Express, 15(20), 13272-13281 (2007).
[24] D. Dey, J. Kohoutek, R. M. Gelfand, A. Bonakdar, and H. Mohseni, "Composite Nano-Antenna Integrated With Quantum Cascade Laser," Ieee Photonics Technology Letters, 22(21), 1580-1582 (2010).
[25] D. Dey, J. Kohoutek, R. M. Gelfand, A. Bonakdar, and H. Mohseni, "Quantum-cascade laser integrated with a metal-dielectric-metal-based plasmonic antenna," Optics Letters, 35(16), 2783-2785 (2010).
[26] H. C. Liu, and F. Capasso, [Intersubband Transitions in Quantum Wells: Physics and Device Applications II] Academic Press, San Diego(2000).
[27] R. Hillenbrand, B. Knoll, and F. Keilmann, "Pure optical contrast in scattering-type scanning near-field microscopy," Journal of Microscopy-Oxford, 202, 77-83 (2001).
[28] E. Cubukcu, N. F. Yu, E. J. Smythe, L. Diehl, K. B. Crozier, and F. Capasso, "Plasmonic Laser Antennas and Related Devices," Ieee Journal of Selected Topics in Quantum Electronics, 14(6), 1448-1461 (2008).
[29] P. R. Griffiths, and J. A. D. Haseth, [Fourier transform infrared spectrometry] Wiley-InterScience, Hoboken, New Jersey(2007).
[30] J. Faist, F. Capasso, C. Sirtori, D. L. Sivco, J. N. Baillargeon, A. L. Hutchinson, S. N. G. Chu, and A. Y. Cho, "High power mid-infrared (lambda greater than or similar to-5 mu m) quantum cascade lasers operating above room temperature," Applied Physics Letters, 68(26), 3680-3682 (1996).
[31] J. Faist, F. Capasso, D. L. Sivco, C. Sirtori, A. L. Hutchinson, and A. Y. Cho, "QUANTUM CASCADE LASER," Science, 264(5158), 553-556 (1994).
[32] C. Gmachl, F. Capasso, D. L. Sivco, and A. Y. Cho, "Recent progress in quantum cascade lasers and applications," Reports on Progress in Physics, 64(11), 1533-1601 (2001).
[33] C. Sirtori, J. Faist, F. Capasso, D. L. Sivco, A. L. Hutchinson, S. N. G. Chu, and A. Y. Cho, "Continuous wave operation of midinfrared (7.4-8.6 mu m) quantum cascade lasers up to 110 K temperature," Applied Physics Letters, 68(13), 1745-1747 (1996).
[34] C. Sirtori, F. Capasso, J. Faist, A. L. Hutchinson, D. L. Sivco, and A. Y. Cho, "Resonant tunneling in quantum cascade lasers," Ieee Journal of Quantum Electronics, 34(9), 1722-1729 (1998).
[35] D. K. Guo, L. E. Cheng, X. Chen, F. S. Choa, J. Y. Fan, and T. Worchesky, "Electrical derivative measurement of quantum cascade lasers," Journal of Applied Physics, 109(4), (2011).
[36] L. A. Coldren, and S. W. Corzine, [Diode Lasers and Photonic Integrated Circuits] John Wiley and Sons, Inc., New York(1995).
[37] C. Gmachl, A. M. Sergent, A. Tredicucci, F. Capasso, A. L. Hutchinson, D. L. Sivco, J. N. Baillargeon, S. N. G. Chu, and A. Y. Cho, "Improved CW operation of quantum cascade lasers with epitaxial-side heat-sinking," Ieee Photonics Technology Letters, 11(11), 1369-1371 (1999).
[38] Y. M. Kim, M. J. W. Rodwell, and A. C. Gossard, "Thermal characteristics of InP, InAlAs, and AlGaAsSb metamorphic buffer layers used in In(0.52)Al(0.48)AS/In0.53Ga0.47As heterojunction bipolar transistors grown on GaAs substrates," Journal of Electronic Materials, 31(3), 196-199 (2002).
[39] D. Dey, W. Wu, O. G. Memis, and H. Mohseni, "Injectorless quantum cascade laser with low voltage defect and improved thermal performance grown by metal-organic chemical-vapor deposition," Applied Physics Letters, 94(8), (2009).